In-line FINCH super resolution digital holographic fluorescence microscopy using a high efficiency transmission liquid crystal GRIN lens

Gary Brooker,[1,2,*] Nisan Siegel,[1,2] Joseph Rosen,[1,2,3] Nobuyuki Hashimoto,[4] Makoto Kurihara,[4] and Ayano Tanabe[4]

[1]*Department of Biomedical Engineering, Johns Hopkins University, 9605 Medical Center Drive, Rockville, Maryland 20850, USA*

[2]*Microscopy Center, Johns Hopkins University Montgomery County Campus, Rockville, Maryland 20850, USA*

[3]*Department of Electrical and Computer Engineering, Ben-Gurion University of the Negev, P.O. Box 653, Beer-Sheva 8410501, Israel*

[4]*Citizen Holdings Co., Ltd., 840 Shimotomi, Tokorozawa 359-8511, Japan*

**Corresponding author: gbrooker@jhu.edu*

Received October 4, 2013; revised November 10, 2013; accepted November 11, 2013; posted November 12, 2013 (Doc. ID 198954); published December 4, 2013

We report a new optical arrangement that creates high-efficiency, high-quality Fresnel incoherent correlation holography (FINCH) holograms using polarization sensitive transmission liquid crystal gradient index (TLCGRIN) diffractive lenses. In contrast, current universal practice in the field employs a reflective spatial light modulator (SLM) to separate sample and reference beams. Polarization sensitive TLCGRIN lenses enable a straight optical path, have >90% transmission efficiency, are not pixilated, and are free of many limitations of reflective SLM devices. For each sample point, two spherical beams created by a glass lens in combination with a polarization sensitive TLCGRIN lens interfere and create a hologram and resultant super resolution image.

OCIS codes: (090.1760) Computer holography; (090.1970) Diffractive optics; (090.1995) Digital holography; (090.2880) Holographic interferometry; (110.0180) Microscopy; (180.6900) Three-dimensional microscopy.

http://dx.doi.org/10.1364/OL.38.005264

Ever since Fresnel incoherent correlation holography (FINCH) [1] showed its potential for fluorescence microscopy [2], we have sought to perfect the technique into a useful high resolution 3D imaging method. The concept that a 3D image could be obtained from incoherent sources by a holographic process, without lasers, scanning or axial translation or the need to capture images at multiple planes of focus to create a 3D image is appealing. The field has now advanced as a result of additional work from ours [3–6] and other laboratories [7–9], including the demonstration that the FINCH optical system is inherently super-resolving [4–6]. Recently it has been shown that FINCH violates the Lagrange invariant [7,10], and this is the basis for its inherent super-resolving properties [11].

Common to all previous studies involving the FINCH technique has been the use of spatial light modulator (SLM) devices to act as in-line beam splitters to separate the reference and sample beams coincident within a single axis (besides the systems suggested by Kim's group [12], which operate like FINCH but are based on a Michelson-like interferometer without a SLM). SLM devices are usually liquid crystal deposited on a reflective semiconductor pixel matrix. Because of the reflective nature of the devices, they must be used at an angle to reflect the processed beam, complicating optical configurations. Furthermore, their resolution is dependent upon the pixel density of the devices and because they are pixelated, light is diffracted into many orders, which significantly reduces light efficiency and results in unwanted image reflections. Even greater light loss is observed if they are used on axis with a beam splitting (BS) cube to try and overcome some of these limitations [3,9]. Other image degrading characteristics include, for example, the small aperture size of the devices, astigmatic properties, and their limited dynamic range. Thus SLM devices inherently reduce light throughput and fidelity, affecting the ultimate resolution of holograms and thus the reconstructed images.

We report here a new high-performance optical system for FINCH that operates in a straight-line optical path with relatively very high transmission efficiency in the creation of the sample and reference beams, and is pixel free and devoid of other limitations of a SLM. The SLM is replaced in this new FINCH configuration with a polarization sensitive transmission liquid crystal gradient index (TLCGRIN) lens [13] in combination with an achromatic glass lens. We previously suggested [4] that a FINCH hologram could be obtained using a glass lens in combination with a SLM to create, from each incoherent sample point, two converging waves, so that an in-line reference and sample beam could interfere and thus create a hologram. Since TLCGRIN lenses are polarization sensitive analog operated electro-optic devices that create high resolution lenses, we were able to adapt them to this new FINCH configuration and overcome the previous functional limitation of SLM-based FINCH devices. In earlier versions of this arrangement we used a TLC Fresnel lens; however, we chose the TLCGRIN lenses because of their tunability and superior optical properties.

The optical setup of this transmission FINCH microscope differs markedly from previous reflection models such that holograms can be captured with high optical efficiency in a straight-line optical setup, while at the same time, the microscope widefield image can be viewed in real time. The reflective SLM function is replaced by the combination of a glass lens and a polarization sensitive TLCGRIN lens. The inefficient plate polarizing filters are replaced by polarizing BS cubes

(Thorlabs CM1-PBS251). The polarizing BS cubes offer almost 100% transmission of each polarization axis and thus yield significantly higher light throughput of the desired polarization. Holograms are captured by CAM1 at the end of the p polarization axis, and the previously wasted s polarization beam is used to view the widefield microscope image through a second camera (CAM2) (or binocular mounted on the first polarizing BS cube). This arrangement allows for the real-time viewing or capture of microscope specimens to focus the microscope or capture comparative widefield images as shown in Fig. 1. In the hologram recording p polarization path, the back aperture of the objective is projected directly onto the tube lens by use of a $4f$ relay [9]. In our current implementation we have taken the additional step of using a magnifying relay with the first relay lens having an $f_1 = 80$ mm focal length while the second relay lens had an $f_2 = 50$ mm focal length. Recall that the FINCH image magnification without the relay unit is z_h/f_o [4–6], and the present overall magnification of the system is $(f_1 z_h)/(f_2 f_o)$, where z_h is the distance between the tube lens and the hologram plane. The relay lenses were achromatic imaging lenses (Rodagon 452341, 452315, respectively) selected to maintain flatness of the image through the relay. The first polarizing BS cube was internal to the relay, and directed the rejected s polarization onto the secondary widefield camera (The Imaging Source DMK23GP031), which was at the focus of the first relay lens. The distance between the relay lenses was corrected for the presence of the BS glass during laser alignment of the system. The tube lens was located at the output focus of the $4f$ relay. Referring to Fig. 1, the sample beam is focused at distance f_{d1} while the reference beam is focused at f_{d2}. The tube lens combines with the active TLCGRIN lens to focus an image at the f_{d1} plane, where $f_{d1} = f_3 f_4/(f_3 + f_4)$, while the f_{d2} plane is focused only by the tube lens at distance f_3. The value of z_h for maximum overlap of the sample and reference beams is fixed by f_{d1} and f_{d2} as follows: $z_h = f_{d1}(1 + s_{\text{fac}}) = f_{d2}(1 - s_{\text{fac}})$, where $s_{\text{fac}} = (f_{d2} - f_{d1})/(f_{d2} + f_{d1})$. We used a variable focal length TLCGRIN lens similar to [13] but with 70 zones, an aperture of 15 mm, a maximum phase stroke of 10 waves, >93% transmission, and a focal range of 5000 mm to infinity (Celloptic and Citizen Holdings). We operated the TLCGRIN lens at its minimum focal length of 5000 mm by driving it with a 1 kHz square wave pulse of about 2 V RMS with 16 bit precision and used a 300 mm 2″ achromatic lens (Thorlabs AC508-300-A) as the tube lens, resulting in f_{d1} of 283 mm, f_{d2} of 300 mm, and z_h of 291.3 mm. This corresponds to a spacing factor s_{fac} of about 0.03, well within the range of optimal spacing of the focal and hologram planes [6]. In addition to the TLCGRIN lens used for creating the hologram, another (inactive) compensating TLCGRIN lens was used, with a fast axis perpendicular to that of the active TLCGRIN lens, to correct for the optical path difference (OPD) in the TLCGRIN lens as is discussed in detail later in this Letter. An electronically variable waveplate (>97% transmission) oriented parallel to the active TLCGRIN lens was used to effect the $2\pi/3$ phase shifts necessary for twin image and zero-order elimination [1–10]. The second polarizing BS cube was positioned after the waveplate, and was polarized parallel to the first BS cube. The hologram recording camera, a Hamamatsu ORCA-Flash 4 CMOS camera, was at the z_h distance of 291.3 mm away from the tube lens. The objective used was a Nikon 20× 0.75 NA. Various microscope filter sets were used (Semrock or Thorlabs) as indicated in the figures, and fluorescent illumination was from a Photofluor II illuminator (89 North) with excitation filters placed in the internal filter wheel and the excitation light delivered to the microscope through a liquid light guide. The signal generators, excitation light source, and cameras were controlled by software written in LabView (National Instruments), in which the calculations were done as well. The TLCGRIN lens voltage was maintained constant to create a predetermined focal length, and the voltage to the liquid crystal phase plate was changed three times to create the required $2\pi/3$ phase shifts during each hologram capture routine. Images were reconstructed from the holograms using methods that have been previously reported [14], and used a Hamming-windowed point spread function for propagation to the reconstruction distance.

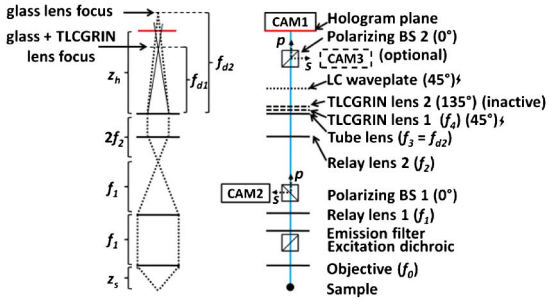

Fig. 1. Schematic of the FINCH fluorescence microscope using TLCGRIN lens. On the left side of the figure is depicted the ray diagram for a FINCH hologram of a point. BS stands for the polarizing beam splitter, and f_0–f_4 are the focal lengths of the objective lens, first and second relay lenses, tube lens, and TLCGRIN lens 1, respectively. TLCGRIN lens 2 is inactive and placed orthogonal to active TLCGRIN lens 1. The sample is located at distance z_s from the objective lens, and the holography camera CAM1 is located at distance z_h from the tube lens, as described in the text. The widefield camera, CAM2 is located at distance f_1 from the first relay lens and views the rejected polarization component (s polarization axis) from the BS1 cube. Distances are corrected to account for the optical path through the glass of the BS cubes. The hologram plane is midway between the focus of the glass tube lens and its reduced focal length due to combination with the polarized component of the TLCGRIN lens. Axis orientation values (in degrees) are given with respect to the p polarization of the first beam splitter.

This new TLCGRIN FINCH configuration maintains the super-resolving properties previously reported using a SLM [4–6]. Figure 2 shows a comparison of TLCGRIN FINCH to the widefield focused image of a fluorescent USAF resolution slide. The smallest group 9 feature linewidth and spacing of 0.78 μm is near the Rayleigh resolution limit of 0.43 μm for the objective NA and emission wavelength. Resolution visibility of 0.4 is seen by standard microscopy with CAM2, and that visibility is approximately doubled, resulting in a super resolution image when the FINCH holograms (captured by CAM1)

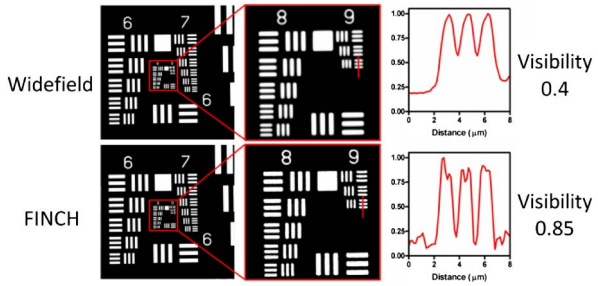

Fig. 2. Fluorescent USAF resolution pattern imaged by widefield (top row) and FINCH fluorescence microscopy (bottom row) with a 20×, 0.75 NA objective, and GFP filter set (525 nm emission). A plastic backing rendered the patterns fluorescent. Left panels are the whole field of view (285 μm on a side), and center panels show enlarged group 8 and 9 features with the smallest features in group 9 approaching the resolution limit. The far-right panels show the line profile intensity through the smallest group 9 features. The visibility with FINCH is increased about twofold when compared to widefield imaging.

are reconstructed to the in-focus plane. In addition, close examination of the images reveals much greater clarity, and the holography exposure times were reduced about fourfold because of better overall light efficiency compared to a SLM system. Pollen grains are more complex objects and were also readily imaged with the new FINCH configuration in both widefield and holography mode; however, only FINCH could reveal the 3D nature of the specimen. Figure 3(a) shows one widefield plane, while Figs. 3(b)–3(d) show multiple planes of focus obtained from the same single hologram captured by FINCH. The FINCH images are of equal or better quality when compared to the widefield image at all planes observed.

As mentioned previously, the TLCGRIN lens used in the current FINCH configuration has birefringent

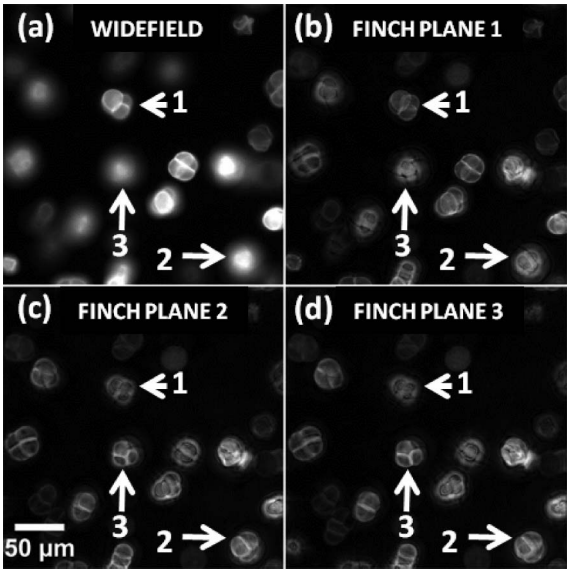

Fig. 3. (a) Widefield and (b)–(d) reconstructed FINCH images of pollen grains captured using a 20× (0.75 NA) objective, showing the ability of FINCH to refocus at depths that were out of focus under widefield conditions. Each full field image is 285 μm square. The widefield image was resampled to match the pixel count of the FINCH images.

properties that can limit the useful bandwidth of the system. Birefringent components in an interferometer, in which the two interfered beams have orthogonal polarizations to each other, create an inherent OPD between the two interfering beams. This OPD puts a limitation on the source bandwidth that can be used in FINCH. However, as we show here, this inherent OPD can be very easily removed. For every birefringent component, the TLCGRIN lens or the phase plate, with ordinary index of refraction n_o, extraordinary index of refraction n_e, and active LC depth d, the OPD between the ordinary and the extraordinary beams is $|n_e - n_o|d$. According to the Wiener–Khintchine theorem, the complex degree of coherence and the source spectrum are a Fourier pair [15]. As the OPD is equal to the product of the coherence time and the light velocity, it is clear that a smaller OPD enables using wider bandwidth light sources for the same value of interference visibility, or for the same level of hologram quality. In other words, in order to get a hologram with good fringe visibility all over its area with a light source of bandwidth $\Delta\lambda$ (in terms of wavelengths), the maximum OPD should satisfy the condition OPD $\leq \lambda^2/\Delta\lambda$ [15,5]. Therefore, for a given OPD, an uncorrected configuration of FINCH is limited to light sources with bandwidth not wider than λ^2/OPD. Considering the birefringent characteristics of the TLCGRIN lens used here, in which $|n_e - n_o| = 0.22$ and $d = 56$ μm, the source bandwidth is limited to be no more than 25 nm. In order to operate the FINCH with wider bandwidth sources, we compensate for, or actually eliminate, the OPD due to the TLCGRIN by introducing into the setup an additional, identical nonactive, TLCGRIN lens rotated by 90° to the active TLCGRIN lens. In that case the two beams with the two orthogonal polarizations pass almost the same optical path after passing the two TLCGRIN lenses. It is "almost" because the ordinary beam, when passing through the active TLCGRIN lens, is modulated by a small perturbation in the index of refraction, but the maximum amplitude of this perturbation is negligible in comparison to n_o. The OPD due to the phase plate should also be corrected. However, because the phase plate is thinner (6.4 μm with the same value of $|n_e - n_o|$), the OPD created by the phase plate is about nine times shorter and therefore has a much less significant effect on system performance than the TLCGRIN lens and at this point has not been corrected by adding an orthogonally polarized phase plate. The effect of adding the orthogonally polarized TLCGRIN lens (Fig. 1 TLCGRIN lens 2) to increase the bandwidth of FINCH is shown in Fig. 4. In the absence of this bandwidth compensation, the visibility of the smallest features in group 9 of the USAF slide began to decline with a bandwidth greater than just 1 nm. However, after compensation, the visibilities were equivalent, within measurement error, up to a bandwidth of 40 nm, more than adequate for fluorescence microscopy. For simplicity we added an inactive TLCGRIN lens to compensate for the birefringence of the active TLCGRIN lens. However, any optics with similar birefringence and thickness could be used.

In the current configuration shown in Fig. 1, the opportunity presents itself to add another holography camera (CAM3 in Fig. 1) to the s polarization output of BS2 and at

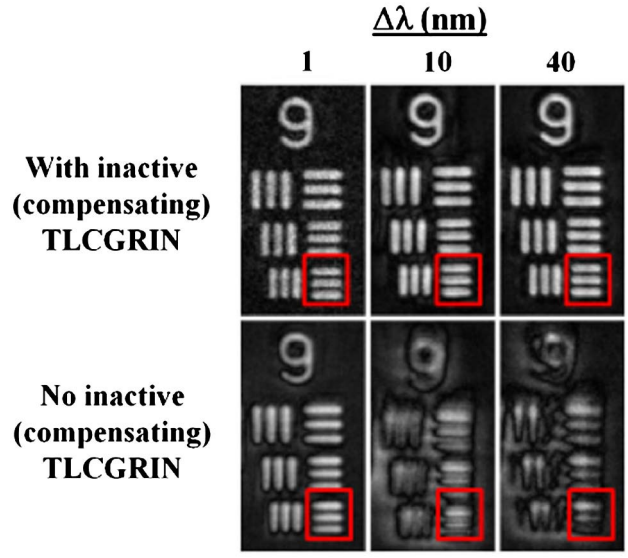

Fig. 4. Effect of bandwidth on visibility of group 9 features in a USAF test slide with and without a compensating TLCGRIN lens placed orthogonal to the active TLCGRIN lens. Top row: with compensation at 1, 10, and 40 nm bandwidth; visibilities were 0.73, 0.65, and 0.69, respectively. Bottom row: without compensation at 1, 10, and 40 nm bandwidth: visibilities were 0.56, 0.26, and 0, respectively.

distance z_h from the tube lens, allowing the number of exposures to obtain a complex FINCH hologram to be reduced from 3 to 2 increasing the temporal resolution of the system. For increased temporal resolution, both holography cameras capture holograms simultaneously to produce four holograms after only two image captures and two phase shifting steps, with each captured hologram having a different phase shift of $\pi/2$ from one another. This is possible because the beam splitting prism transfers vector components from the ordinary and the extraordinary axes, two projected onto the p axis and two onto the s axis. It is easy to see that if the p axis contains the sum of the ordinary and extraordinary components, the s axis contains the difference of those components and vice versa. The final effect is that the two holograms captured simultaneously are phase shifted π from each other. The fringe patterns recorded on both cameras are identical except for the phase difference of π between them. Therefore, when the phase angle on the phase plate is 0, the hologram in CAM3 is shifted by π (a half cycle of the fringes) in comparison to the hologram recorded by CAM1. However, when the phase angle on the phase plate is $\pi/2$, the hologram in CAM1 is shifted by $\pi/2$ (a quarter cycle of the fringes) in comparison with the hologram recorded by the same camera in the first exposure. The hologram on CAM3 is shifted by $3\pi/2$ in comparison with the same hologram recorded in CAM1 in the first exposure. In conclusion, for increased temporal resolution there are four raw holograms with four steps of phase shift, 0, $\pi/2$, π, and $3\pi/2$, taken only from two exposures, but that yield together, after a simple, well-known digital superposition, a complex-valued hologram that is as good as the hologram obtained with three exposures and three phase shifts. By doing this we shorten exposure time and illumination of the sample by 1/3 without compromising hologram quality. The second optional camera can also be used to increase the signal-to-noise ratio (S/N) over using a single hologram camera in the mode where three exposures are used to create a complex hologram. The complex holograms from each camera are simultaneously recorded without increasing exposure time. In this case, using the second camera can increase the light efficiency by a factor of 2 and the S/N by the square root of the number of complex holograms.

This work was supported by NIST ARRA Award 60NANB10D008, NIH Grant U54GM105814, The Israel Ministry of Science and Technology, The Israel Science Foundation, and CellOptic, Inc.

References

1. J. Rosen and G. Brooker, Opt. Lett. **32**, 912 (2007).
2. J. Rosen and G. Brooker, Nat. Photonics **2**, 190 (2008).
3. G. Brooker, N. Siegel, V. Wang, and J. Rosen, Opt. Express **19**, 5047 (2011).
4. J. Rosen, N. Siegel, and G. Brooker, Opt. Express **19**, 26249 (2011).
5. B. Katz, J. Rosen, R. Kelner, and G. Brooker, Opt. Express **20**, 9109 (2012).
6. N. Siegel, J. Rosen, and G. Brooker, Opt. Express **20**, 19822 (2012).
7. P. Bouchal, J. Kapitan, R. Chmelik, and Z. Bouchal, Opt. Express **19**, 15603 (2011).
8. X. Lai, Y. Zhao, X. Lv, Z. Zhou, and S. Zeng, Opt. Lett. **37**, 2445 (2012).
9. P. Bouchal and Z. Bouchal, J. Eur. Opt. Soc. Rapid Pub. **8**, 13011 (2013).
10. X. Lai, S. Zeng, X. Lv, J. Yuan, and L. Fu, Opt. Lett. **38**, 1896 (2013).
11. R. Kelner, J. Rosen, and G. Brooker, Opt. Express **21**, 20131 (2013).
12. M. K. Kim, Opt. Express **21**, 9636 (2013).
13. N. Hashimoto and M. Kurihara, Proc. SPIE **7232**, 72320N (2009).
14. N. Siegel, J. Rosen, and G. Brooker, Opt. Lett. **38**, 3922 (2013).
15. M. Born and E. Wolf, *Principles of Optics* (Cambridge, 1999), Chap. 10.3.2, p. 566.